Lidar-activated Phosphors and Infrared Retro-Reflectors: Emerging Target Materials for Calibration and Control

J. Anderson, R. Massaro, L. Lewis, R. Moyers, and J. Wilkins

Introduction

Lidar

Lidar, or Light Distance and Ranging, has become a fast and accurate means to acquire dense digital renderings of the terrain including detailed elevation and topographic models. These data support a wide variety of applications varying from photogrammetry to remote sensing and are seen as a rapidly developing tool for cost-effective mapping. It has been shown, point-for-point, that lidar can be as or more cost-effective in topographic mapping than traditional surveying methods. This is certainly the primary reason lidar is enjoying unprecedented growth and success as a mapping and remote sensing technology (Flood and Gutelieus, 1997; Flood, 2001).

Established almost 30 years ago, the concept of using lasers to accurately measure distances was initiated by the National Aeronautics and Space Administration (NASA). Two instruments developed by the agency in the1980s and incorporated as deployable airborne laser rangefinder instruments demonstrated the utility of "laser altimetry" or the pre-cursor to lidar. These instruments were the Atmospheric Oceanographic Lidar (AOL) and Airborne Topographic Mapper (ATM). The mapping accomplished by these systems successfully demonstrated not only from a variety of airborne platforms, but from near-Earth orbits during the Shuttle Laser Altimeter (SLA) missions. These systems incorporated pulsed lasers and time gating for effective measurement and accurate acquisition of elevations. NASA has since expanded airborne and space-based lidar missions incorporating laser altimetry to measure vegetation canopies as well as provide detailed images and topographic maps of Mars via the Mars Observer Laser Altimeter (MOLA) (Flood, 2001).

Terrestrial applications of lidar have ranged from forest canopy mapping, flood and hazards analysis and landform surveys to accurate bathymetric profiling. In each case, lidar systems possessing different wavelengths are selected to record the elevation or depth (in bathymetric applications) of features. Typically, lidar operates within eye-safe ranges and power levels in the visible or near- to short-wave infrared region of the electromagnetic spectrum. Furthermore, lidar can be classified into two broad operational categories based upon the wavelength, pulse, divergence and illumination area of the laser. Lefsky *et al.* describe these as: 1) discrete return or 2) waveform sampling (Lefsky *et al.*, 2002). These categories represent technologies that are distinguished in part by the size of the laser illumination area, or footprint. The laser footprint is typically smaller with discrete return systems (0.25–1 m) than with waveform sampling systems (10–100 m) (Hudak *et al.*, 2002). Waveform sampling systems are characterized by their coarse horizontal resolution, but compensate for this attribute with finer vertical resolution, providing sub-meter vertical profiles (Lefsky *et al.*, 2002). Discrete return systems are characterized by their ability to record only one to five returns per laser footprint. In this regard, discrete return systems are better suited for supplying the current production demands for accurate, high-resolution topographic maps and digital terrain models, and are therefore widely available in the commercial sector (Lefsky *et al.*, 2002). However, Hug *et al.* (2004) have described RIEGL's Litemapper 5600 as one of the first commercial full waveform digitization lidars capable of collecting full surface information as well as topographic content. With near infinite returns possible per pulse, the user-selected target detection characteristics are limitless in post-processing. Waveform sampling systems have been highly useful in forest canopy research and applications, such as biomass assessments in temperate (Lefsky *et al.*, 1999; Harding *et al.*, 2001) and tropical forests (Drake *et al.*, 2002).

continued on page 876

continued from page 875

Lidar Targets and Materials

Lidar applications continue to expand with both current and emerging systems representing both discrete and full waveform capabilities that yet promise higher accuracy and broader coverage. As these systems evolve, the use of in-scene targets for controlling geometric fidelity or marking objects of interest in-scene becomes an application for active remote sensing. Lidar offers a unique way to not only measure topographic information or characterize surface structures, but (as an excitation source) stimulate materials placed within a particular area for a variety of applications from target tracking to environmental monitoring (Anderson *et al.*, 2007). Recently, lidar target research has been actively initiated by the mapping community for the accurate rendition of roads and corridors. Toth *et al.*, (2008) describe the use of pavement retro-reflective materials and lidar for providing accurate measurement of ground control in highways. Csanyi *et al.*, (2005) describe the need for, and fabrication procedures of, specific targets for lidar to enhance accuracy and serve as in-scene references. They argue that the delicate complexity of the sensory components (GPS, INS, and laser range-finder) required for accurate measurements introduce errors that must be compensated for in lidar data. Furthermore, they argue that post-processing alone cannot account for the errors in control and that in-scene targets are an area of research necessary to represent known horizontal and vertical positions. However, these investigations consider the necessary spatial attributes of target function, i.e., matching target size to point density. What is left is the consideration of the target material itself and the return stimulated by the excitation pulse that is identifiable in intensity *above* the background.

Materials capable of being stimulated by lidar fall into two categories: retro-reflectors and phosphors. Retro-reflectors ideally return most or all incident light falling upon them to their source with a minimum of scattering. Many retro-reflective materials are emerging with high refractive indices in excess of 1.8 or greater. With such efficiencies, these materials incorporated into lidar targets should provide for high quality in-scene calibration and geometric control. Moreover, research in these materials will not only benefit lidar mapping and remote sensing, but also may serve recent advances in the use of free-space optics for the efficient transmitting and receiving of telecommunications data (Goetz *et al.*, 2003).

Luminescent phosphors or phosphor crystals as a target material offer visible or short-wave infrared emissions subsequent to the absorption of a lidar pulse. These materials can be formulated to produce an array of colors at many operational lidar wavelengths through the up-conversion process (Anderson *et al.*, 2007). The up-conversion mechanism effectively doubles the photon flux through electron saturation of certain materials that in turn doubles the long wavelength excitation producing a short wavelength emission (e.g., lidar stimulation at 1064 nm produces a green emission at 532 nm). In our research, phosphor crystals are specifically synthesized suitable to lidar stimulation (i.e., possessing high quantum efficiencies) and are based on calcium or strontium lattices doped with rare earth ions such as europium (Eu^+) or samarium (Sm^+). These crystals emit visible radiation subsequent to the absorption of a lidar pulse through a process known as optical stimulated luminescence. In this regard, the activation of these materials can be recorded using visible multi- or hyper-spectral imagery or observed in the lidar point cloud as an absorption in the intensity data.

With the emergence of new lidar technologies, lidar target development should enjoy the same innovational trajectory. Furthermore, while retro-reflective materials (e.g., corner cube reflectors and cat's eye optics) offer one approach in lidar targeting, we are engaged in the investigation of selective, high efficiency reflectors as well as up-conversion materials that absorb lidar, but re-emit this energy as electro-optic-based visible or near infrared light. We present here our work in characterizing novel materials that can selectively reflect or absorb lidar wavelengths and the implications for improving lidar target applications for sensing, calibration and correction.

Emerging Materials

Retro Reflectors

For our targeting experiments we are investigating the use of 30 μm diameter Barium Titinate (BaTiO3) glass beads incorporated into a variety of target designs. In larger forms, these materials are typically found in road and highway paints and reflective optics. To be suitable for lidar calibration and targeting, we have found that the bead size controls the optimal return associated with its refractive index. Beads larger or smaller than 30 μm do not necessarily return as efficiently when using lidar as the incident excitation source. In our selection of BaTiO3 glass beads, a theoretical model of their retro-reflective properties, (i.e., their ability to reflect light back along the direction of the incident illuminating beam) has been applied. Since our selected target area presented to the lidar excitation is only 12 cm in diameter, the retro-reflective properties of the beads have been a critical factor in predicting the necessary return against a complex background such as terrain within a point cloud.

The retro-reflective properties of select beads have been evaluated as a function of the bead's refractive index, internal specular reflection in accordance with Snell's law, and diffuse reflection from a coating on the wall of the bead. Given a uniform ray of light propagating parallel to the x-axis is incident on a single sphere, as shown in Figure 1-left. Light incident on the surface of the sphere will behave in accordance

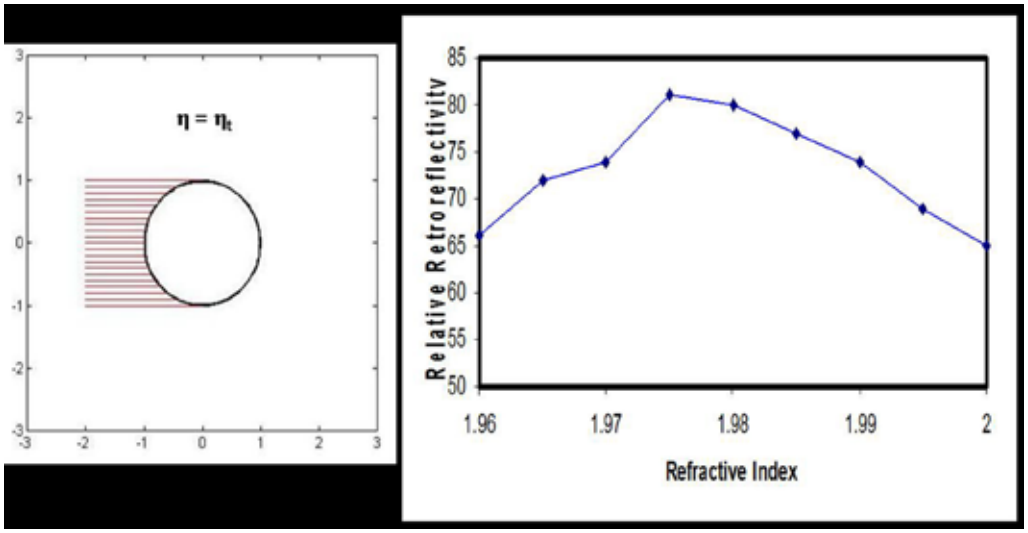

Figure 1. Uniform light impinging on a retro-reflective bead (left) and a model of retro-reflective efficiency as a function of refractive index (right). (models courtesy Dr. Richard Moyers, Oak Ridge National Labs)

with Snell's law $\eta_i \sin\theta_i = \eta_t \sin\theta_t$, where η_i is the index of refraction of the incident medium (air, η_i=1), and η_t is the index of refraction inside the bead. θ_i is the angle of the incident light relative to the sphere surface normal, and θ_t is the angle of the refracted beam. Snell's law predicts that some of the incident light will be reflected by the front surface of the sphere, and the rest will be refracted toward the rear surface. Light that reaches the rear surface will again experience reflectance and refraction at the surface. Most of the light is transmitted out of the bead, but about 15% of the light will be reflected off the surface back toward the front surface of the bead. The model indicates that, depending on the refractive index, 9% - 12% of the light originally incident upon the bead will be transmitted out of the sphere and retro-reflected back towards the incident light source. A plot of reto-reflected intensity as a function of bead refractive index is shown in Figure 1-right. The plot shows that the model indicates that a bead index of 1.977 should provide optimal retro-reflectivity and thus be easily recovered in a complex point cloud representing a variety of terrain features and backgrounds.

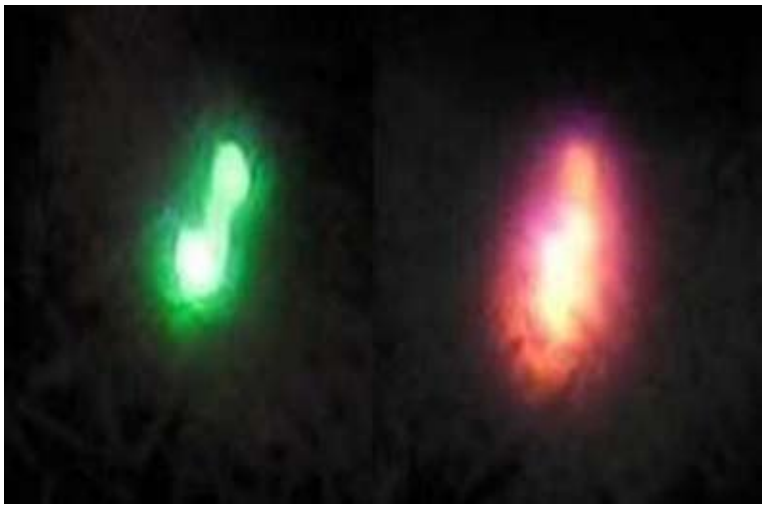

Figure 2. Up-converting crystals absorbing lidar short-wave energy and re-emitting at visible wavelengths.

Phosphors

In our research, phosphor crystals are specifically synthesized suitable to lidar stimulation (i.e., possessing high quantum efficiencies) and are based on calcium or strontium lattices doped with rare earth ions such as europium (Eu^+) or samarium (Sm^+). These crystals emit visible radiation subsequent to the absorption of a near infrared (1064 nm) lidar pulse through a process known as optically-stimulated luminescence (Figure 2.). In this regard, the activation of these materials can be recorded using visible multi- or hyperspectral imagery or observed in the lidar point cloud as an absorption in the intensity data.

The conversion of near-infrared photons to higher energy states (UV or visible light) via multiple absorptions or energy transfer, is known as up-conversion. In up-converting materials, energy is stored in a quasi-stable excited state known as an "electron trap". Electron traps are created by rare earth ions synthesized in the crystal particles. When the NIR light is absorbed by the up-converting material, the energy is raised to a higher, more unstable excited state. A visible wavelength photon is emitted as the material relaxes from the unstable excited state to the ground state. Figure 3 presents spectral measurement on the up-conversion process showing broadly emitted red light (610 to 630 nm) from a crystal excited by an Optech 1064 nm laser source.

Other phosphor research we are conducting, as applied to lidar, focuses on crystal compound synthesis and doping using elemental (ytterbium) Yb^{3+} as a sensitizer. Due to the specific electron transitions and high quantum yields (> 0.7) associated within such compounds, it is possible to excite the particle crystal with low energy NIR lasers to obtain bright red, green and even blue emissions. This is important as the ground energy of lidar is inherently weak, and weaker still upon detection at the receiving optics. We have also explored the induction of up-conversion at other wavelengths, specifically 1500 nm, by utilizing sensitizers other than Yb^{3+}. The absorption spectrum of (erbium) Er^{3+} show significant absorption at 1.5 µm due to specific electron transitions making it an ideal eye-safe sensitizer. By co-doping with either (homium or terbium) Ho^{3+} or Tm^{3+}, energy transfer from the excited Er^{3+} induces a two-photon absorption resulting in green (550 nm) or infrared (800 nm) emissions, respectively.

Lidar Materials Evaluation

Recent testing on these material types was conducted at Fort A.P. Hill, Virginia using a modified Optech ALTM 3100/Gemini lidar system. The system operates between 33 to 167 kHz pulse repetition rate (33000 to 167000 light pulses per second) and at a variety of altitudes ranging from 800 to 3500m. The scan rate, pulse rate, and altitude were chosen to achieve a variety of independent point spacing (i.e., resolution) on the ground. The resulting target data collected were captured using the ALTM's four channel, analog timing measurement circuit, which was capable of recording four returns for each transmitted laser pulse (first, second, third, and last). The airborne platform used in this experiment was a King Air A90 aircraft operated by Dynamic Aviation, Staunton, Virginia. To evaluate the materials effectively, two lidar configurations were used – standard mapping and target modes. For mapping, the ALTM was mounted inside the aircraft to enable a standard nadir mapping that allowed an unobstructed field of view (FOV) of +/- 20 degrees. This is consistent with the scan mirror range of the lidar sensor. To enable target mode collection, the sensor was mounted in a specially

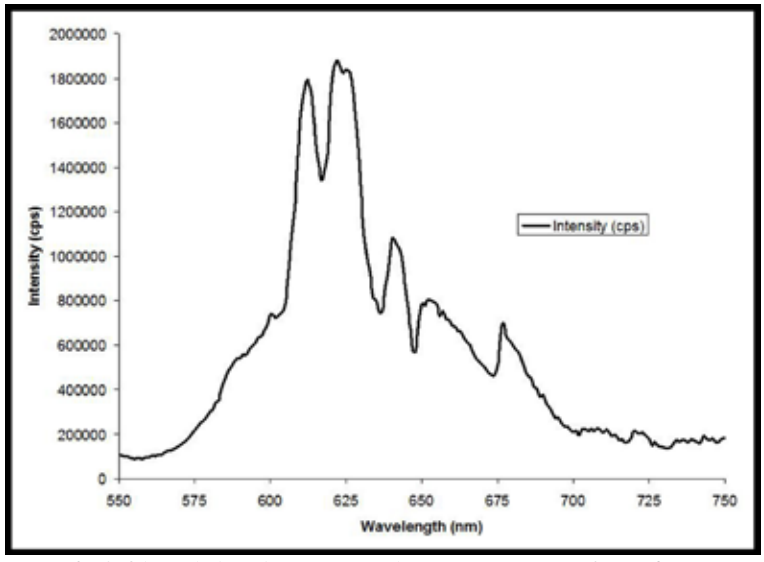

Figure 3. CaS-based phosphor emission due to up-conversion from 1064 nm lidar excitation.

continued on page 878

continued from page 878

designed two-axis gimbal with a stabilized pointing system. This gimbal can provide an additional +/- 30 degrees of motion about each axis when mounted in a suitably configured aircraft. Target mode permits the continuous scanning of an area (typically 50 m by 50 m) enabling the materials to be exposed to a greater number of laser pulses from the lidar. At various altitudes, this permitted an evaluation of the materials as a function of laser energy and increased beam divergence.

The normal, minimum eye-safe operating altitude of the lidar is 640 m above ground level. For our tests, we started with an altitude of 171 m to get as much laser energy on the ground as possible. To further maximize the laser energy per pulse, the system was operated at the minimum laser pulse rate of 33 kHz. Finally, thirty-one passes comprised a typical test sortie with altitudes of 171, 201, 238, 274, and 335 m.

Lidar and Materials

In our evaluation of these materials we have observed that both types possess attributes useful to in–scene lidar calibration and targeting. High refractive index retro-reflective optics as those described, show definitive waveform characteristics and are highly distinguishable above complex backgrounds. In addition, the phosphor materials tested also demonstrated waveform characteristics useful for targeting. Furthermore, these materials demonstrate useful absorptive and emissive properties related to their up-converting characteristics. Both material types have promising attributes for calibration and control within acquired lidar scenes when used as the optical components of targets. Figure 4 shows the intensity point cloud over a test matrix established at Fort A.P. Hill, Virginia. Also presented are the target material's associated waveforms against the background and Enhanced CCD (EMCCD) imaging data showing the lidar excitation pulse and its interaction with the targets (Figure 5). The visible emission of the phosphor materials subsequent to the absorption of the lidar in the target test field is well-documented by the imagery as well as strong retro-reflective returns.

Figure 6 shows the waveform characteristics of the material types and the measured waveforms each possesses against the background. In the case of the retro-reflective beads integrated into targets, the return is 10-fold. Phosphors exhibit returns just above the ground exhibiting absorption of the lidar beam. Given these attributes, each material demonstrates qualities desirable in effective calibration targets within the lidar point cloud. Furthermore, these materials should exhibit more detailed signature characteristics in full waveform lidar data with its expanded radiometric range and greater sensed returns per pulse.

Conclusion

The integration of emerging, highly efficient retro-reflective and phosphorescent optical materials into lidar remote sensing should help expand the technology from standard topographic range finding to active remote sensing. While literature has shown that the majority of the up-converting materials operate at 980 nm, we have shown that we can effectively expand their use to work with wavelengths commonly employed in lidar applications, specifically 1500 nm (eye-safe) as well as 1064 nm. We also feel the integration of up-conversion materials in lidar remote sensing may eventually serve as a reporter technology, observable by co-mounted multi- or hyperspcetral sensing systems. This may permit environmental probes or monitoring devices to be placed in-scene and triggered by lidar permitting ground conditions to be monitored and mapped effectively.

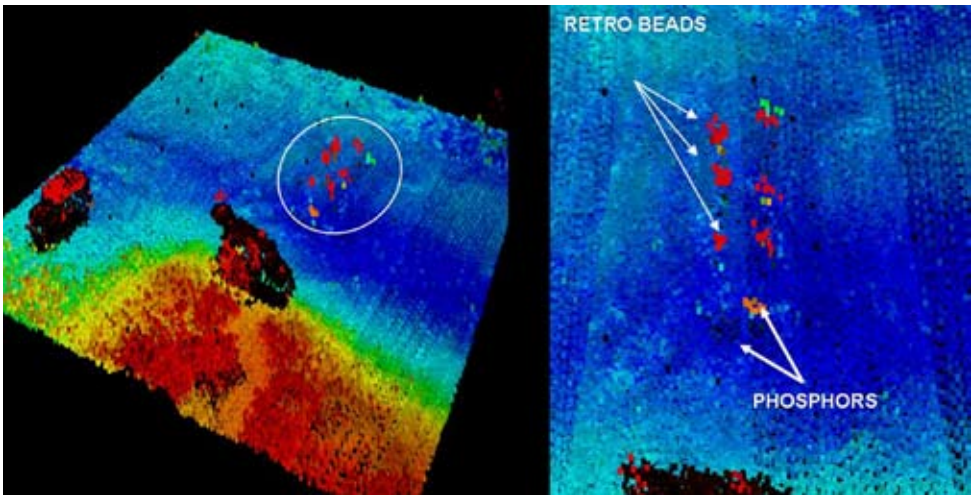

Figure 4. (Left) Optech ALTM lidar point cloud of Retro and Phosphor test matrix at Fort A.P.Hill, Virginia, August 2009. (Right) Close up view of materials stimulated by lidar using multiple point clouds in mapping mode from sorties at 274 meters.

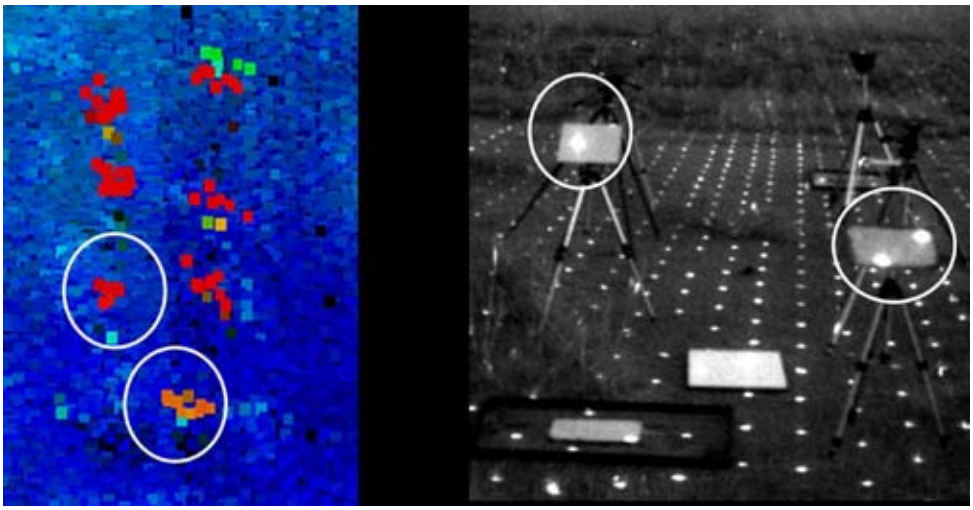

Figure 5. Comparative point cloud (left) and EMCCD data (right) for Phosphor – P and Retro- reflective – R target materials. The unfiltered EMCCD data recorded both the lidar point density, 1064 nm refection of the retros and phosphors and visible emission for the phosphors.

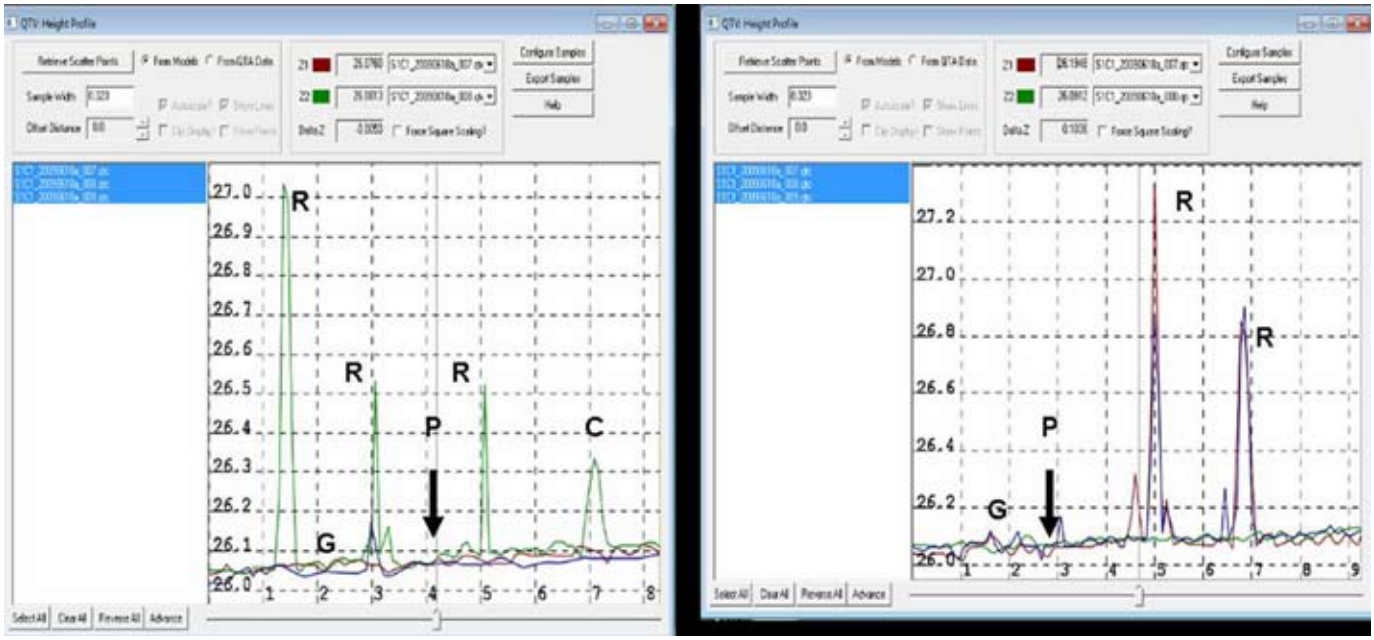

Figure 6. Left and Right plots of range resolution waveform characteristics of retro and phosphor targets showing: saturation by retro-reflectors -R, Spectralon calibration panel-C and absorption in waveforms by phosphors (P) as compared to the ground (G).

With regard to retro-reflective optics, we have found that the BaTiO3 beads are highly versatile and adapt readily to a variety of target configurations. The importance of these materials is that they can be distributed in small quantities or integrated into small targets and still be separated from complex backgrounds. The spectral structure and intensity waveform characteristics of these materials makes them easy to separate from backgrounds, a critical requirement for calibration and in-scene control. Finally, further research is ongoing to fuse both technologies to enhance multi-sensory approaches where lidar is the principle excitation source.

Literature Cited

Anderson, J., R. Massaro, J. Edwards, G. Glaspell, W. Bernard, O. Weatherbee, 2008. Hyperspectral fluorescence remote sensing of landscape molecular probes, In Proc. *ASPRS 2008 Annual Conference Portland, Oregon 2008*. April 23 – May 2, 2008.

Csanyi, N., C. Toth, D. Brzezinska, J. Ray, 2002. Improvement of lidar data accuracy using lidar specific ground targets, In Proc. *ASPRS 2005 Annual Conference Baltimore, Maryland*, March 7-11, 2005.

Drake, J., R. Dubayah, D. Clark, R. Knox, J. Blair, M. Hofton, R. Chazdon, J. Weishample, S. Prince, 2002. Estimation of tropical forest structural characteristics using large-foorprint lidar, *Remote Sensing of Environment,* 79:305-319.

Flood, M., Gutelius, B., 1997. Commercial implications of topographic terrain mapping using scanning airborne laser radar, *Photogrammetric Engineering and Remote Sensing*, 63(4), pp. 327-329 and 363-366.

Flood, M., 2001. Commercial lidar technology: The next five years, in Proc. *ASPRS Annual Conference 2001,* (St. Louis).

Goetz, P., W. Rabinovich, T. Meehan, D. Katzer, S. Binari, E. Funk, C. Gilbreath, 2003. Modulating retroreflector implementation of MILSTD 1553 protocol with free-space optics, In Proc. *IEEE Aerospace Conference* 2003, Paper No. 1559.

Harding, D., M. Lefsky, G. Parker, J. Blair, 2001 lidar altimeter measurements of canopy structure: Methods and validation for closed canopy, broadleaved forests, *Remote Sensing of Environment,* 76:283-297.

Hudak, A., M. Lefsky, W. Cohen, M. Berterretche, 2002. Integration of lidar and Landsat ETM+ data for estimating and mapping forest canopy height, *Remote Sensing of Environment,* 70: 339-361.

Hug, C., A. Ullrich, A. Grimm, 2004. Litemapper 5600 – a waveform-digitizing lidar terrain and vegetation mapping system, *ISPRS,* Vol. XXXVI, 8/W2.

Lefsky, M.A., W.B. Cohen, S.A. Acker, G.G. Parker, T.A. Spies, and D. Harding, 1999. Lidar remote sensing of the canopy structure and biophysical properties of Douglas-fir western hemlock forests, *Remote Sensing of Environment,* 82: 397-416.

Lefsky, M.A., W. Cohen, G. Parker, D. Harding, 2002. Lidar remote sensing for ecosystem studies, *Bioscience,* 52, 1; pg. 19.

Toth, C. , E. Paska, D. Brzezinska, 2008. Using road pavement markings as ground control for lidar data, *ISPRS,* Vol. XXXVII, Part B1, Beijing 2008.

Author

John E. Anderson, Ph.D.
Senior Research Biologist – Remote Sensing
US Army Corps of Engineers, Engineer Research and Dev. Center
Alexandria, Virginia 22315
john.anderson@usace.army.mil, (w) 703-428-6698

Co-Authors

R. Massaro and **J. Wilkins**
US Army Corps of Engineers, Engineer Research and Dev. Center
Alexandria, Virginia 22315

L. Lewis and **R. Moyers**
US Department of Energy, Oak Ridge National Laboratories
1060 Commerce Park Drive, Oak Ridge, TN 37830

Opening image — IKONOS imagery provided courtesy of Space Imaging. Lidar derived elevation map courtesy of USGS and NASA